NALM-based, phase-preserving 2R regenerator of high-duty-cycle pulses

Taras I. Lakoba[1*], **Jake R. Williams**[1], **and Michael Vasilyev**[2]

[1]*Department of Mathematics and Statistics, University of Vermont, Burlington, VT 05401*
[2]*Department of Electrical Engineering, University of Texas at Arlington, Arlington, TX 76019*
[*]*Corresponding author: tlakoba@uvm.edu*

Abstract: We explore the potential of the nonlinear amplifying loop mirror (NALM)-based phase-preserving 2R (reamplification and reshaping) regenerator for simultaneous regeneration of multiple wavelength-division-multiplexed (WDM) channels. While not considering nonlinear multi-channel propagation, we address two issues of the phase-preserving NALM that appear to us as the major obstacles in adopting it for realistic WDM applications: a high operating power and a detrimental effect of non-small (33% – 50%) pulse duty cycles. After thorough optimization, we find a new operating regime of this regenerator with the non-small duty-cycle capability and approximately an order of magnitude reduction of the required operating power. In addition, we show that the plateau in the input–output power transfer curve does not automatically lead to the reduction of the amplitude jitter, which is particularly noticeable for the non-small duty-cycle pulses.

OCIS codes: (060.2330) Fiber optics communications; (060.4510) Optical communications; (070.4340) Nonlinear optical signal processing; (230.1150) All-optical devices; (230.4320) Nonlinear optical devices.

References and links

1. K. Croussore, C. Kim, G. Li, "All-optical regeneration of differential phase-shift keying signals based on phase-sensitive amplification," Opt. Lett. **29**, 2357–2359 (2004).
2. R. Slavik, F. Parmigiani, J. Kakande, C. Lundstrom, M. Sjodin, P. A. Andrekson, R. Weerasuriya, S. Sygletos, A. D. Ellis, L. Gruner-Nielsen, D. Jakobsen, S. Herstrom, R. Phelan, J. O'Gorman, A. Bogris, D. Syvridis, S. Dasgupta, P. Petropoulos, D. J. Richardson, "All-optical phase and amplitude regenerator for next-generation telecommunications systems," Nature Photon. **4**, 690–695 (2010).
3. M. Matsumoto, H. Sakaguchi, "DPSK signal regeneration using a fiber-based amplitude regenerator," Opt. Express **16**, 11169–11175 (2008).
4. A. G. Striegler, M. Meissner, K. Cvecek, K. Sponsel, G. Leuchs, B. Schmauss, "NOLM-based RZ-DPSK signal regeneration," IEEE Photon. Technol. Lett. **17**, 639–641 (2005).
5. S. Boscolo, R. Bhamber, and S.K. Turitsyn, "Design of Raman-based nonlinear loop mirror for all-optical 2R regeneration of differential phase-shift-keying transmission," IEEE J. Quantum Electron. **42**, 619–624 (2006).
6. M. Matsumoto, "Performance improvement of phase-shift-keying signal transmission by means of optical limiters using four-wave mixing in fibers," J. of Lightwave Technol. **23**, 2696–2701 (2005).

7. Q. T. Le, L. Bramerie, H. T. Nguyen, M. Gay, S. Lobo, M. Joindot, J.-L. Oudar, and J.-C. Simon, "Saturable-absorber-based phase-preserving amplitude regeneration of RZ DPSK signals," IEEE Photon. Technol. Lett. **22**, 887–889 (2010).
8. A. Fragkos, A. Bogris, D. Syvridis, R.Phelan, J. O'Carroll, B.Kelly, and J.O'Gorman, "Amplitude regeneration of phase encoded signals using injection locking in semiconductor lasers," *Optical Fiber Communication Conference*, Optical Society of America, 2011, Technical Digest on CD-ROM, paper OWG1.
9. G.P. Agrawal, *Nonlinear Fiber Optics*, 3rd Ed. (Academic Press, San Diego, CA, 2001); Chap. 7.
10. K. Sponsel, K. Cvecek, C. Stephan, G. Onishchukov, B. Schmauss, G. Leuchs, "Optimization of a nonlinear amplifyAing loop mirror for amplitude regeneration in phase-shift-keyed transmission," IEEE Photon. Technol. Lett. **19**, 1858–1860 (2007).
11. T.I. Lakoba, J.R. Williams, M. Vasilyev, "Low-power, phase-preserving 2R amplitude regenerator," submitted for publication; preprint is available at http://www.cems.uvm.edu/~lakobati/recent_publications/2011_MismatchedCoupler.pdf .
12. A. Bogoni, M. Scaffardi, P. Gelfi, L. Poti, "Nonlinear optical loop mirrors: investigation, solution, and experimental validation for undesirable counterpropagating effects in all-optical signal processing," IEEE J. Sel. Top. Quantum Electron. **10**, 1115–1123 (2004).
13. M. Vasilyev and T. I. Lakoba, "Fiber-based all-optical 2R regeneration of multiple WDM channels," in *Optical Fiber Communication Conference*, Optical Society of America, 2005, Technical Digest on CD-ROM, paper OME62.
14. T.I. Lakoba, M. Vasilyev, "A new robust regime for a dispersion-managed multichannel 2R regenerator," Opt. Express **15**, 10061–10074 (2007).
15. M. Eiselt, "Does spectrally periodic dispersion compensation reduce non-linear effects?" in *Proceedings of the 25th European Conference on Optical Communications* (ECOC, Nice, France, 1999), Vol. **1**, pp. 144–145.
16. X. Wei, X. Liu, C. Xie, and L. F. Mollenauer, "Reduction of collision-induced timing jitter in dense wavelength-division multiplexing by the use of periodic-group-delay dispersion compensators," Opt. Lett. **28**, 983–985 (2003).
17. M. Vasilyev and T. I. Lakoba, "All-optical multichannel 2R regeneration in a fiber-based device," Opt. Lett. **30**, 1458–1460 (2005).
18. G. Bellotti and S. Bigo, "Cross-phase modulation suppressor for multispan dispersion-managed WDM transmission," IEEE Photon. Technol. Lett. **12**, 726–728 (2000).
19. L. F. Mollenauer, A. Grant, X. Liu, X. Wei, C. Xie, and I. Kang, "Experimental test of dense wavelength-division multiplexing using novel, periofic-group-delay-complemented dispersion compensation and dispersion-managed solitons," Opt. Lett. **28**, 2043–2045 (2003).
20. P.G. Patki, M. Vasilyev, T.I. Lakoba, "All-optical regeneration of multi-wavelength signals," in *IEEE/LEOS European Winter Topical on Nonlinear Processing in Optical Fibres*, IEEE 2009, pp. 254–255.
21. C. Stephan, K. Sponsel, G. Onishchukov, B. Schmauss, G. Leuchs, "Phase preserving amplitude regeneration in DPSK transmission systems using a nonlinear amplifying loop mirror," IEEE J. Quantum Electron. **45**, 1336–1343 (2009).
22. K. Sponsel, K. Cvecek, C. Stephan, G. Onishchukov, B. Schmauss, G. Leuchs, "Influence of group velocity dispersion on phase-preserving amplitude regeneration by a nonlinear amplifying loop mirror," in *Conference on Lasers and Electro-Optics*, Optical Society of America, 2008, Technical Digest on CD-ROM, paper JWA95.
23. C. K. Madsen, G. Lenz, A. J. Bruce, M. A. Cappuzzo, L. T. Gomez, R. E. Scotti, "Integrated all-pass filters for tunable dispersion and dispersion slope compensation," IEEE Photon. Technol. Lett. **12**, 1623–1625 (1999).
24. C. R. Doerr, L. W. Stulz, S. Cbandrasekhar, L. Buhl, R. Pafchek, "Multichannel integrated tunable dispersion compensator employing a thermooptic lens," *Optical Fiber Communications Conference 2002*, post-deadline paper FA-6.
25. R. L. Lachance, S. Lelievre, and Y. Painchaud, "50 and 100 GHz multi-channel tunable chromatic dispersion slope compensator," *Optical Fiber Communications Conference*, Optical Society of America, 2003, Technical Digest, paper TuD3.
26. K. Cvecek, K. Sponsel, G. Onishchukov, B. Schmauss, G. Leuchs, "2R-regeneration of an RZ-DPSK signal using a nonlinear amplifying loop mirror," IEEE Photon. Technol. Lett. **19**, 146–148 (2007).

1. Introduction

Growing popularity of the phase-encoded modulation formats (e.g. differential phase-shift keying, or DPSK, and differential quadrature-shift keying, or DQSK) in long-haul transmission systems has lead to the need for development of all-optical regenerators capable of processing these formats. Strictly speaking, phase regeneration requires the use of either phase-sensitive amplifiers [1, 2] or phase-to-amplitude demodulation [3]. However, in most cases it is sufficient to employ simpler, phase-*preserving*, amplitude regenerators, which suppress both amplitude jitter and the dominant phase noise originating from the amplitude-to-phase noise conversion by a medium with Kerr nonlinearity. A number of such phase-preserving amplitude regenerator schemes have been recently proposed and demonstrated [4]–[8]. To make these regenerators practically useful, however, one needs to adapt them to wavelength-division multiplexing (WDM) operation, where many WDM channels are processed by a single regenerator. Such an adaptation is fundamentally impossible for schemes [6]–[8] relying on gain saturation, but feasible, at least in principle, for the scheme [4, 5] based on self-phase modulation in a nonlinear amplifying loop mirror (NALM).

In this paper we explore the potential of the NALM-based regenerator [4] to simultaneously regenerate multiple WDM channels. This requires a clarification: we do *not* study here the multi-channel operation of this device, postponing such a study to a separate publication. Instead, we address two issues of the setup of [4] which appear to us as the major obstacles in adopting it for realistic WDM applications. These issues — a high operating power and a detrimental effect of non-small (33% – 50%) pulse duty cycle — are described in Secs. 2 and 3, respectively, and their resolution is proposed and demonstrated in Sec. 4.

2. Operating power of a NALM-based regenerator

The setup of a NALM-based regenerator is shown in Fig. 1; see Sec. 4 for its detailed description. Regenerating properties of this device are due to power dependence of the phases of the signals propagating in the opposite directions inside the NALM and interfering at its output. In the absence of dispersion of the highly nonlinear fiber (HNLF), these phases are [9]:

$$\phi_{\rm cw} = \gamma L(P_{\rm cw} + 2G\overline{P_{\rm ccw}}), \tag{1a}$$

$$\phi_{\rm ccw} = \gamma L(GP_{\rm ccw} + 2\overline{P_{\rm cw}}). \tag{1b}$$

Here subscripts ‘cw’ and ‘ccw’ stand for clock- and counterclockwise propagating signals, P and $\overline{P}$ are the peak and time-averaged powers, and γ and L are the nonlinearity and length of the HNLF. The first and second terms in each of Eqs. (1) are due to self- and cross-phase modulation (SPM and XPM), respectively. In Eqs. (1) and in the rest of this paper we ignore any polarization effects.

For phase-encoded signals with pulse duty cycle d and no amplitude jitter, the time-averaged and peak powers are related as

$$\overline{P} = Pd. \tag{2}$$

The output power and phase of the regenerated signal are [4, 10, 11]:

$$P_{\text{out}} = GP_{\text{in}}|\alpha e^{i\phi_{\text{cw}}} - (1-\alpha)e^{i\phi_{\text{ccw}}}|^2, \tag{3a}$$

$$\phi_{\text{out}} = \phi_{\text{in}} + \arg\left[\alpha e^{i\phi_{\text{cw}}} - (1-\alpha)e^{i\phi_{\text{ccw}}}\right] - 2\gamma L(\overline{P}_{\text{cw}} + G\overline{P_{\text{ccw}}}), \tag{3b}$$

$$P_{\text{cw}} = \alpha P_{\text{in}}, \qquad P_{\text{ccw}} = (1-\alpha)P_{\text{in}}, \tag{3c}$$

where α is the power splitting ratio of the coupler (see Fig. 1).

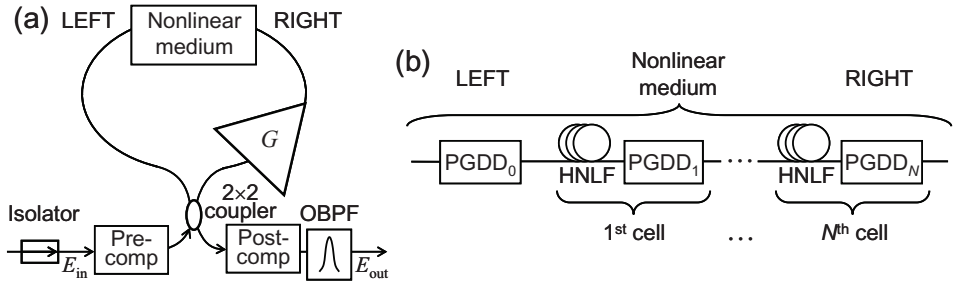

Fig. 1. (a) Schematics of a NALM-based regenerator. (b) Details of the nonlinear medium.

In Fig. 2 we plot representative power transfer curves for such values of α and d where those curves and the corresponding phase transfer curves, $\phi_{\text{out}} = \phi_{\text{out}}(P_{\text{in}})$, have plateaus over overlapping intervals of input power [4]. In studies of 2R regeneration it is widely accepted that a device operating at a plateau of a power transfer curve cleans up amplitude jitter of the signal. In Sec. 3 we will show that for a NALM-based regenerator this is not necessarily the case, but for now we will proceed accepting the aforementioned role of a plateau. Then from Fig. 2 one sees that the output power is on the order of several Watts. Moreover, it increases with d, so that for $d = 0.50$ it gets "pushed to infinity", and the plateau disappears. This effect is caused by XPM-induced terms in (1). A similar detrimental effect of XPM for high duty-cycle pulses was noted earlier in [12] in a somewhat different setup.

High operating power of a NALM-based regenerator presents a number of obstacles for its WDM applications. First, nonlinear interaction among high-power channels is likely to distort the signals so that it would offset any improvement brought about by regeneration. Second, a flat-gain amplifier inside the NALM required for such high-power signals could be very expensive. Third, and not specific to WDM, only several milliwatts of the regenerated signal can be re-launched into the communication line. The remaining power, i.e. more than 99% of it, will have to be wasted.

Thus, the first issue that we will address in Sec. 4 is lowering the operating power of the regenerator. We will demonstrate that it is possible to reduce the power requirements by almost an order of magnitude compared to Fig. 2. Further power reduction is possible if one replaces the conventional coupler of the NALM by one with considerable amounts of propagation constant mismatch and asymmetric dissipation in the two cores, which we have recently proposed in [11]. It should be noted that a different method of lowering the operating power was proposed in [12] (see also [10] for a related result). In this method, the XPM that causes the operating

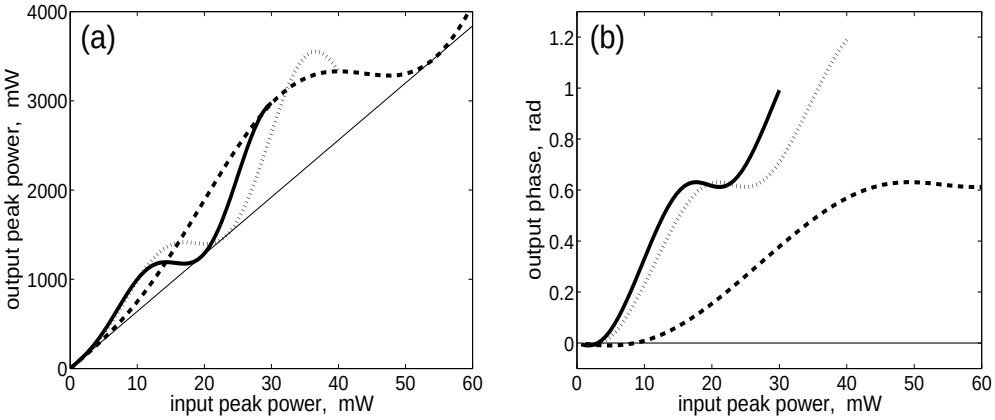

Fig. 2. Power (a) and phase (b) transfer curves of a dispersionless regenerator with total nonlinearity parameter $\gamma L = 37.5$ W^{-1} and employing input pulses of varying duty cycle d. Thick solid: $d = 0.025$; dotted: $d = 0.10$; dashed: $d = 0.33$; thin solid: $d = 0.50$. In all cases, the coupler's splitting ratio is at its (nearly) optimal value $\alpha = 0.90$.

power increase is counteracted by adjustment of a polarization state of the signal. However, active polarization control would be impractical for a multi-channel application of the regenerator. In contrast, the low-power regime presented in Sec. 4 does not rely on polarization control.

3. Effect of pulse duty cycle on amplitude jitter reduction

As we mentioned, the presence of a plateau as in Fig. 2 is usually interpreted as the ability of the device to reduce amplitude jitter of the input signal. Indeed, if a transfer curve $P_{\text{out}} = f(P_{\text{in}})$ has a plateau near $P_{\text{in}} = P_0$, then $f(P_0 + \Delta P) \approx f(P_0)$ for all sufficiently small ΔP, which is tantamount of amplitude jitter suppression. Below we demonstrate that the above logic does not work for a NALM unless the pulse duty cycle is sufficiently small (which is not the case in practice where $d \geq 0.33$). That is, a plateau in a transfer curve of a NALM does *not* guarantee suppression of amplitude jitter.

In Fig. 3a we show the power-transfer characteristic of a NALM with parameters described in the next section, except that the average dispersion of the nonlinear dispersive medium is 10 ps/nm/km, the width of the PGDD filter (see Sec. 4) is 100 GHz, and $d = 33\%$. Even though all pulses at the input for each simulated P_{in} nominally have the same input peak power, it actually fluctuates slightly from pulse to pulse due to finite bandwidth of the data modulator and the interference of the fields of adjacent pulses. These slight fluctuations at the input are transformed into the output power fluctuations. The two solid curves in Fig. 3a depict the corresponding maximum and minimum powers of the output signal. These curves are in close proximity with each other, which in analogy with the Mamyshev regenerator suggests [13, 14] that the NALM should suppress amplitude jitter.

However, this is not the case. In Fig. 3a the dashed lines show the maximum and minimum output powers of the same NALM when the input pulses have power jitter of $\pm 10\%$. The output

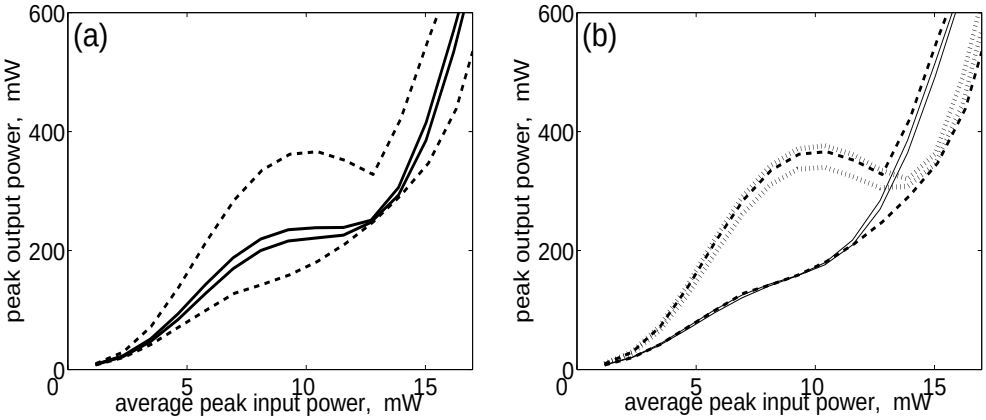

Fig. 3. Power transfer curves of a regenerator with the parameters listed in the text. (a) Solid lines: input with no amplitude jitter; dashed: input with $\pm 10\%$ jitter. (b) Dashed: same as in (a); solid (dotted): first (second) numerical experiment described after Table 2.

power jitter is higher than $\pm 30\%$ for those input powers which correspond to the plateau in the solid curves. We will explain below that this occurs due to XPM caused by the counterpropagating signal in the NALM (see Eqs. (1)).

To begin, consider a jitterless input for which the power-transfer curve has a plateau. The instantaneous output power is some function of the instantaneous input power and the time-averaged power of the counterpropagating part of the signal; see Eqs. (1) and (3). Note that the instantaneous and time-averaged powers, P and $\overline{P}$, affect the output power separately. Then one can write

$$P_{\text{out}} = F(P_{\text{in}}, \overline{P_{\text{in}}}) \tag{4a}$$

for some nonlinear function $F(x_1, x_2)$. Note that for a signal *with amplitude jitter*, P and $\overline{P}$ are *not* related by (2), and so (4a) cannot be simplified any further. However, for *jitterless* signals, which are commonly used to compute transfer curves, P and $\overline{P}$ *are* related by (2), so that:

$$\underline{\text{for jitterless signal only:}} \qquad P_{\text{out}} = F(P_{\text{in}}, P_{\text{in}} d). \tag{4b}$$

Let $P_{\text{in}} \equiv X$ be somewhere inside the plateau of the transfer curve. Then (4b) takes on the form of the first line of Table 1. The second and third lines of that Table correspond to jitterless inputs with powers $(1 \mp 0.1)X$. The approximate equalities $(\approx Y)$ in the right column there hold because we assume that all three input powers, X and $(1 \mp 0.1)X$, are in the plateau of the transfer curve.

Now consider an input with $\pm 10\%$ amplitude jitter, such that the peak powers fluctuate between $0.9X$ and $1.1X$, but the time-averaged power is Xd. The corresponding output powers are listed in the right column of Table 2. Note that the output powers in the last two lines of that Table are not, in general, close to $F(X, Xd) = Y$. It is this fact that explains the strong output

Peak input power	Time-averaged input power	Output power
X	Xd	$F(X,Xd)\equiv Y$
$0.9X$	$0.9Xd$	$F(0.9X,0.9Xd)\approx Y$
$1.1X$	$1.1Xd$	$F(1.1X,1.1Xd)\approx Y$

Table 1. Output power schematics for a jitterless input.

Peak input power	Time-averaged input power	Output power
X	$1\cdot Xd$	$F(X,1\cdot Xd)\equiv Y$
$0.9X$	$\mathbf{1}\cdot Xd$	$F(0.9X,\mathbf{1}\cdot Xd)=???$
$1.1X$	$\mathbf{1}\cdot Xd$	$F(1.1X,\mathbf{1}\cdot Xd)=???$

Table 2. Output power schematics for an input with $\pm 10\%$ jitter.

jitter shown by the dashed lines in Fig. 3a. The higher the duty cycle d, the stronger this effect, because the greater the absolute difference between $1\cdot Xd$ and either $1.1Xd$ or $0.9Xd$ (i.e., the second argument of F).

To verify the above explanation, we designed the following numerical experiment. First, we simulated propagation of a *jitterless* input through a NALM where we *adjusted by hand* the counterpropagating power to equal $(1/0.9)\overline{P_{\rm in}} \equiv (1/0.9)P_{\rm in}d$. This situation corresponds to the second line of Table 2. Then we expect that the lower of the pair of the transfer curves in this case is to coincide with the lower transfer curve in the case where the input has $\pm 10\%$ jitter. The above reference to the *lower* of the pair of curves assumes that $F(x_1,x_2)$ is an increasing function of the first argument, x_1.

Similarly, we also simulated a jitterless input where the counterpropagating power was adjusted by hand to correspond to $(1/1.1)\overline{P_{\rm in}}$. (This imitates the third line in Table 2.) In this case we expect that the upper of the pair of curves is to coincide with the upper transfer curve for the input with 10% jitter. (Again, by referencing the *upper* curve we have assumed that $F(x_1,x_2)$ is an increasing function of x_1.) A comparison between our expectation and numerics is shown in Fig. 3b, where the solid (dotted) curves correspond to the first (second) numerical experiment. The agreement is good up to a power corresponding to the right end of the plateau in Fig. 3a. For higher powers, a "cross-over" occurs, whereby one of the curves for the first (second) experiment gets aligned with the *upper* (*lower*) curve in the case with 10% jitter. Such a cross-over simply indicates that $F(x_1,x_2)$ ceases to be an increasing function of x_1 for the higher input powers, but does not contradict our explanation illustrated by Tables 1 and 2. Moreover, we conducted similar experiments for other parameter values and found that our explanation was upheld by them as well. Incidentally, the cross-over does not always occur: for example, it

was found not to occur for an ASK-, instead of DPSK-, modulated signal, with the rest of the parameters being the same as listed above. (The difference between the ASK and DPSK cases here is the ratio $\overline{P}/P$, which is given by (2) for DPSK but is twice as small for the ASK case.)

We have demonstrated that the presence of a plateau in the power transfer curve does not guarantee suppression of amplitude jitter by a NALM-based regenerator. Below we propose a different, simple method to find a regime guaranteeing such suppression. One simulates propagation of an input pulse sequence having some amplitude jitter (we used $\pm 20\%$) and plots the two transfer curves, for the the minimum and maximum output powers, $P_{\mathrm{out,min}}$ and $P_{\mathrm{out,max}}$, similar to Fig. 3. The ratio

$$(P_{\mathrm{out,max}} - P_{\mathrm{out,min}})/(P_{\mathrm{out,max}} + P_{\mathrm{out,min}}) \tag{5}$$

is the output jitter. Whenever it is less than the input jitter, we declare that the device has suppressed amplitude jitter.

Since we are ultimately concerned with the ability of the NALM to increase the eye opening of *phase-encoded* signals, we also monitor the phase-transfer curve, $\phi_{\mathrm{out}} = \phi_{\mathrm{out}}(P_{\mathrm{in}})$, and accept only those cases where the output phase varies little with the input power. Our approach is illustrated in the next section.

4. Low-power regimes of phase-preserving amplitude jitter suppression

In the first part of this section we will use the approach described above to identify regeneration regimes mentioned in this section's title. Then in the second part, we will verify that the eye opening improvement in these regimes is similar to that for the NALM-based regenerator using low duty-cycle pulses, studied earlier.

4.1. Power and phase transfer curves

We begin by specifying parameters of the setup shown in Fig. 1. Two types of the 2×2 coupler were considered. The first was the conventional coupler used in all previous studies of a NALM. This coupler is uniquely characterized by its power-splitting ratio, $\alpha = P_{\mathrm{cw}} : P_{\mathrm{ccw}}$ (see Eqs. (1)). The other was a modified coupler, by employing which one can considerably lower the operating power of a NALM-based regenerator [11]. This modified coupler has propagation constant mismatch between its two cores, as well as dissipation in one of the cores. The corresponding parameters will be introduced later on when we present results pertaining to this type of coupler.

Gain G of the amplifier inside the NALM was fixed at 20 dB in all the simulations reported below. In principle, regeneration can be observed at values of G as low as 17 dB [10] and 3 dB [11] with the conventional and modified couplers, respectively. (The input power is then correspondingly higher.) However, we did not explore regimes with $G \neq 20$ dB in detail so as not to defocus this study.

The optical bandpass filter (OBPF) at the output of the NALM was chosen as a second-order Gaussian with its central frequency coinciding with that of the signal. The shape and bandwidth of the OBPF were chosen so as to make the shape and temporal width of output and input pulses

approximately the same. Thus, everywhere except at the very end of Sec. 4.2, its full width at half maximum (FWHM) is taken as 25 GHz. Pre- and post-compensations of dispersion were provided before and after the NALM, as shown in Fig. 1a.

The nonlinear medium consists of N identical cells composed of an HNLF section of length L and a periodic group-delay device (PGDD). The nonlinearity and dispersion coefficients of the HNLF are $\gamma = 5$ (W·km)$^{-1}$ and $D = -120$ ps/nm/km. The PGDD is a key component that enables considerable reduction of detrimental nonlinear interaction among multiple WDM channels; this has been demonstrated both numerically [15]–[17] and experimentally [18]–[20]. Since, as we announced in the Introduction, in the future we plan to extend the setup reported here to multi-channel operation, it is natural to include PGDDs in it. However, in this paper we only consider single-channel propagation, and hence it is relevant to mention only two properties of the PGDD: (i) its dispersion $\mathscr{D}_{\text{PGDD}}$ partially compensates dispersion of the HNLF section:

$$DL + \mathscr{D}_{\text{PGDD}} \equiv D_{\text{av}} L, \tag{6}$$

and (ii) it has a bandpass filtering characteristic. The latter will play an important role in the regimes reported below and will be referred to as a "PGDD filter". It is modeled as third-order Gaussian with FWHM values reported below. In this study we ignored the loss of HNLF and PGDDs; they will be included in a future study concerned with multi-channel modeling.

The first and last PGDD, PGDD$_0$ and PGDD$_N$ (see Fig. 1b), were allowed to be different from the inline PGDDs given by (6). However, we found that the regenerator performance was determined not by $\mathscr{D}_0$ and $\mathscr{D}_N$ individually, but (approximately) by parameter combinations

$$(\mathscr{D}_N + \text{pre-compensation}) \qquad \text{and} \qquad (\mathscr{D}_0 + \text{post-compensation}). \tag{7}$$

Therefore we fixed $\mathscr{D}_0$ and $\mathscr{D}_N$ to some specific values: $\mathscr{D}_0 = 1.5\mathscr{D}_{\text{PGDD}}$ and $\mathscr{D}_N = -0.5\mathscr{D}_{\text{PGDD}}$, without loss of generality.

The input pulses in the simulations reported below had repetition rate 10 Gb/s and duty cycle $d = 50\%$. We chose it over another practical value, $d = 33\%$, for two reasons. First, finding a regeneration regime for the higher duty cycle (i.e., 50% instead of 33%) emphasizes the difference of such a regime from the low duty-cycle regime ($d = 2.5\%$) studied earlier (see [21] and references therein). To justify the validity of comparison between these two regimes, note that the regime considered in [21] is not dispersionless, as it used 2.5-ps pulses in a fiber with $D = -2$ ps/nm/km. However, it was shown in [22] to have the operating power similar to that in the dispersionless case. Now recall from Fig. 2 that in the dispersionless case, regeneration is impossible for $d = 50\%$ at any power. Thus, our finding of a low-power regeneration regime for $d = 50\%$ provides the most contrast to the earlier studied case [21].

Our second reason for choosing $d = 50\%$ was that in the future we plan to verify our numerical results experimentally, and therefore we used the duty cycle of the transmitter available in the lab of the third co-author (M.V.). The pulse shape at the transmitter is modeled as

$$E(t) = E_0 \sin\left[\frac{\pi}{4} - \frac{\pi}{4}\cos\left(\frac{2\pi t}{T_{\text{bit}}}\right)\right], \tag{8}$$

where T_{bit} is the duration of the bit slot.

Thus, in our search of a regime where the NALM-based regenerator suppresses amplitude jitter of high duty-cycle pulses, we varied the following parameters: the number N of 'HNLF+PGDD' cells; average dispersion $D_{\rm av}$ of each cell; length L of the HNLF section; power-splitting ratio α of the conventional coupler (or three parameters listed below for a modified coupler); FWHM of the PGDD filter; and pre- and post-compensation of dispersion (see Fig. 1b). For each set of these values we obtained a pair of power and phase transfer curves for an input with $\pm 20\%$ amplitude jitter, as described in Sec. 3. Such curves corresponding to (nearly) optimal jitter suppression are shown in Fig. 4, where the conventional coupler was used in the NALM.

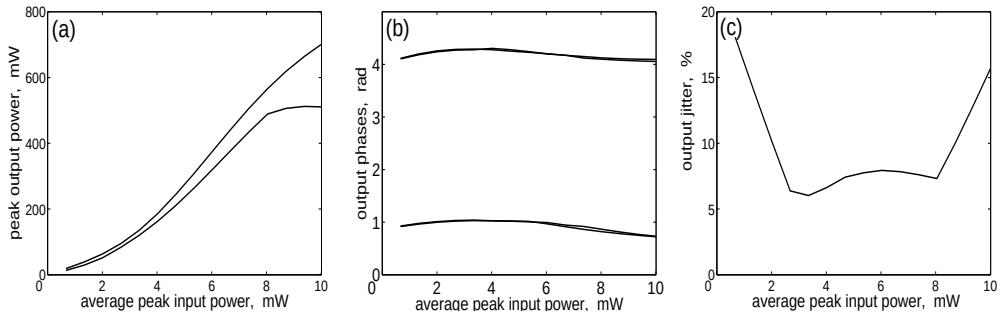

Fig. 4. Power (a) and phase (b) transfer curves, and output jitter (c). In (b), the curves are shown for both ONEs and ZEROs. Parameters not listed in the text are: $D_{\rm av} = 5$ ps/nm/km, $\alpha = 0.75$, PGDD filter's FWHM is 50 GHz, and pre- and post-compensations are -200 and 200 ps/nm.

An analogous result for the NALM with a modified coupler is shown in Fig. 5. The fields $\mathscr{E}_{1,2}$ in the two cores of the coupler safisfy:

$$\begin{aligned} \partial_z \mathscr{E}_1 &= i\Delta \mathscr{E}_1 + i\kappa \mathscr{E}_2 \\ \partial_z \mathscr{E}_2 &= i\kappa \mathscr{E}_1 - (i\Delta + \mu)\mathscr{E}_2 \,, \end{aligned} \tag{9}$$

where ∂_z denotes the derivative with respect to the distance z along the coupler, κ and Δ are the coupling and mismatch between the cores, and μ is the dissipation present only in the second core [11]. Values of parameters κz_c (where z_c is the coupler's length), Δ/κ, and μ/κ for the regime with optimal jitter suppression are listed in the caption to Fig. 5.

A few comments are in order about the results presented in these figures. First, we found that, in general, the regenerator's performance improves when we increased the number of cells N. However, this would also increase the cost of the device, and hence here we report the minimum number, $N = 6$, for which we found good performance. The HNLF length that gives good results in this case is $L = 1.25$ km. Second, the performance is only slightly affected if the pre- and post-compensations are varied within 50 ps/nm of their optimal values.

Our last two comments are about the role and feasibility of experimental realization of a PGDD with filter bandwidth of ~ 50 GHz. In modern 10-Gb/s telecommunication systems

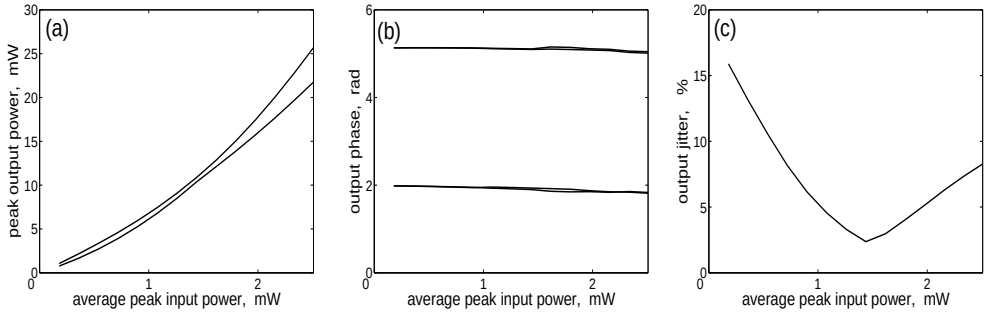

Fig. 5. Same as in Fig. 4, but for a modified coupler with $\kappa z_c = 1.4$, $\Delta = \kappa$, and $\mu = 0.6\kappa$. Also, $D_{\text{av}} = -5$ ps/nm/km, and pre- and post-compensations are -100 and 200 ps/nm.

channel separation can be 50 GHz or even less. However, in analogy with our earlier studies of a multi-channel Mamyshev regenerator [14, 17], we expect that multi-channel operation of the NALM-based regenerator will require at least 200 GHz of channel separation. Thus, a 50-GHz filter characteristic would occupy only about 25 % of the interchannel spacing provided by the PGDD; i.e., it is *narrow*. A PGDD with such a narrow-band filtering is easier to fabricate than a higher-bandwidth one [23]–[25]. It is, therefore, fortunate that jitter suppression requires just such a narrow PGDD filter. As one widens it, e.g., even to only 70 GHz, the regenerator performance becomes considerably worse.

4.2. Eye opening (EO) improvement

To quantify the EO improvement provided by the regenerator, we simulated propagation of a 10-Gb/s pseudo-random bit sequence of length $2^7 - 1$, which had a $\pm 30\%$ amplitude jitter and no phase jitter. We compared three cases. Case (i) is similar to the one modeled in [21, 26]: we used *uniform* HNLF (with no PGDDs) with $D = -2$ ps/nm/km, $L = 2$ km, and $\gamma = 2.5$ (W·km)$^{-1}$. The differences from [21, 26] are that we used 5-ps pulses instead of 2.5-ps ones and also correspondingly adjusted the coupler's splitting ratio to be $\alpha = 0.86$ instead of 0.80. The average peak input power was 220 mW. No pre-compensation was used in this case, and the entire dispersion of the HNLF, i.e. -4 ps/nm, was compensated at the receiver. There was no optical filter at the receiver, and the electrical filter's FWHM was 75 GHz. The input and regenerated eye diagrams are shown in Figs. 6a,b. The EO improvement with respect to a 1-ps "window" fitted inside the electrical eye is 1.3 dB, in good agreement with the result (1.2 dB) reported in [26].

Case (ii) was suggested by the results of Fig. 4. Namely, we used $N = 6$ 'HNLF + PGDD' cells with the HNLF parameters of $L = 1.25$ km, $D = -120$ ps/nm/km, and $\gamma = 5$ (W·km)$^{-1}$, and the cell's average dispersion $D_{\text{av}} = 5$ ps/nm/km. The PGDD filter's bandwidth was 50 GHz; the coupler's splitting ratio $\alpha = 0.75$. The pulses had $d = 50\%$ (see (8)), and the average peak input power was 6.8 mW. The pre- and post-compensations were -200 and 200 ps/nm. The optical and electrical filters' bandwidths at the receiver were 40 and 7.5 GHz. The

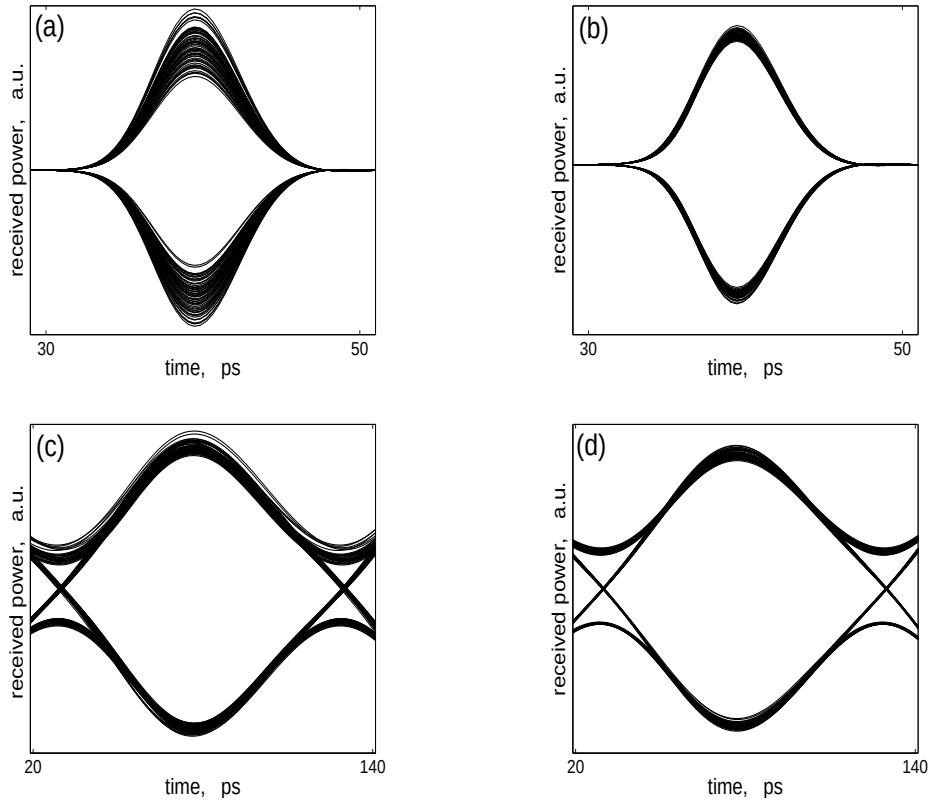

Fig. 6. Electrical eye diagrams of the input (a) and outputs in cases (i)–(iii) (panels (b)–(d), respectively).

EO improvement with respect to a 10-ps "window" fitted inside the electrical eye is 1.1 dB; see Fig. 6c. Finally, case (iii) was similar to case (ii) except that: a modified coupler with parameters $\kappa z_c = 1.4$, $\Delta = \kappa$, and $\mu = 0.6\kappa$ was used; $D_{\text{av}} = -5$ ps/nm/km; the pre- and post-compensations were -100 and 200 ps/nm; and the average peak input power was 1.4 mW. The EO improvement in this case is 1.0 dB; see Fig. 6d.

It is worth mentioning that the optimal amplitude jitter suppression inferred from results such as those presented in Figs. 4c and 5c does not guarantee an optimal EO improvement. A competing factor is the broadening of the output pulse compared to the input one, which can partially undo the jitter suppression benefit. This is why the EO in case (ii) is slightly higher than in case (iii), even though Figs. 4c and 5c indicate that the jitter suppression is stronger in the latter case. Similarly, this is also why we reported case (ii) for the input power of 6.8 mW, corresponding to the right-hand side of the "well" in Fig. 4c, rather than for the lower power of 3–4 mW corresponding to the left-hand side of the "well".

Finally, we verified that the lower-power regimes found above are robust with respect to moderately small variations of the device parameters and the average signal power. Specifically, EO improvement of at least 1.0 dB was observed when in case (ii), one had: $0 \leq D_{\text{av}} \leq 10$

ps/nm/km, $0.72 \leq \alpha \leq 0.78$, PGDD filter's FWHM between 40 and 50 GHz, and the average peak input power between 6.46 and 7.14 mW (i.e., 6.8 mW $\pm 5\%$). At $D_{\text{av}} = 0$ the performance slightly sagged, which we were able to counteract by using a precompensation of -100 ps/nm; the postcompensation in this case remained at 200 ps/nm. In a case similar to (iii), where a modified coupler is used, we found that EO improvement of at least 1.0 dB (with a peak value of 1.2 dB) was observed when: the OBPF at the output of the NALM had FWHM of 45 GHz, $0 \leq D_{\text{av}} \leq 10$ ps/nm/km, PGDD filter's FWHM was between 40 and 50 GHz, the average peak input power was 1.3 mW $\pm 10\%$, and the parameter Δ/κ was within an interval at least as large as $[0.98, 1.02]$ when $\kappa z_c = 1.4$ and $\mu = 0.6\kappa$. We did not investigate the robustness of the low-power regime with an EO improvement exceeding 1.0 dB while varying the latter two parameters, but it is likely that they also can be varied by at least $\pm 2\%$ each (in addition to the other parameters varying as stated above).

5. Conclusions

In this paper we obtained two main results. First, in Sec. 3, we showed that a plateau of a power transfer curve of a regenerator based on a loop mirror implies amplitude jitter suppression *only*, in general, for low duty-cycle signals. This occurs because of the counterpropagating field's in the loop affecting, via XPM, any given pulse. More specifically, the effect of the counterpropagating field is proportional to the *time-averaged* power, which in a signal with amplitude jitter is *not* related to the *instantaneous* pulse power. This effect is stronger for high duty-cycle pulses because, for a given peak power, they have a higher time-averaged power.

To our knowledge, the fact that a plateau in the power transfer curve does not automatically entail jitter suppression has not been noted in the existing literature. Moreover, we emphasize that the main mechanism of poor (or even negative) jitter suppression observed in this work is *not*, unlike that in, e.g., [13], the interaction of adjacent pulses. Indeed, adjacent pulses of shape (8) do not overlap in the absence of dispersion, and the dispersion of one HNLF section — approximately -150 ps/nm — could not have caused any significant broadening to a 50-ps pulse. Rather, in this work, the main contributor to poor jitter suppression in the presence of a plateau of the power transfer curve is XPM, as explained above.

Our second main result is finding a relatively low-power regeneration regime for high duty-cycle pulses when the NALM has a distributed nonlinear dispersive medium (see Fig. 1). A direct comparison of the operating powers in this low-power regime (see, e.g., Fig. 4) and in the dispersionless case having the same total nonlinearity (see Fig. 2) cannot be made because in the dispersionless case, regeneration is impossible at any power for 50% duty-cycle pulses that we used. Therefore, we compare the regime of Fig. 4 with that for 33% duty-cycle pulses in Fig. 2 and observe more than a six-fold reduction of the input power (from more than 40 mW to 6.8 mW). Thus, roughly speaking, the input power is almost an order of magnitude less than it could have been inferred from the dispersionless case. A further five-fold reduction of the operating power can be achieved by the use of a modified coupler proposed in [11]; see Fig. 5 and the last paragraph in Sec. 4.2.

Finding a low-power regime required optimization of many parameters of the NALM. How-

ever, the most important for the existence of this regime seems to be the distributed narrow-band filtering provided by PGDDs.

We plan to study multi-channel operation of a NALM-based regenerator with 'HNLF + PGDD' cells in a future publication.

Acknowledgement

This work was supported in part by the NSF grants ECCS-0925706 and ECCS-0925860.